Key Engineering Materials
ISSN: 1662-9795, Vol. 784, pp 9-14
doi:10.4028/www.scientific.net/KEM.784.9

Submitted: 2017-12-30
Accepted: 2018-06-06
Online: 2018-10-29

Microstructure and Local Mechanical Properties of Skutterudites with Addition of Metallic Borides

Jiří Buršík[1,a]*, Vilma Buršíková[2,b], Gerda Rogl[3,4,c] and Peter Rogl[3,d]

[1]Institute of Physics of Materials, Czech Academy of Sciences, Žižkova 22, CZ-61662 Brno, Czech Republic

[2]Department of Physical Electronics, Faculty of Science, Masaryk University, Kotlářská 2, CZ-61137 Brno, Czech Republic

[3]Institute of Materials Chemistry and Research, University of Vienna, Währingerstr. 42, A-1090 Wien, Austria

[4]Institute of Solid State Physics, Vienna University of Technology, Wiedner Hauptstr. 8-10, A-1040 Wien, Austria

[a]bursik@ipm.cz, [b]vilmab@physics.muni.cz, [c]gerda.rogl@univie.ac.at, [d]peter.franz.rogl@univie.ac.at

Keywords: thermoelectrics, skutterudite, nanoindentation, microstructure

Abstract. Skutterudites are an important class of thermoelectric p- and n-type materials and they have already achieved fair efficiencies for the conversion of heat to electricity. Nevertheless researchers try to further enhance the figure of merit, ZT, by various ways. In this work we study microstructure and mechanical properties of two thermoelectric materials: an industrial n-type $(Mm,Sm)_yCo_4Sb_{12}$ skutterudite and an industrial p-type $DD_yFe_3CoSb_{12}$ skutterudite, both mixed with 1 wt.% of $Ta_{0.8}Zr_{0.2}B$. Thin lamellae were prepared from the compacted materials using a focused ion beam. Analytical transmission electron microscopy was used on lamellae to study details of microstructure. A fine dispersion of precipitates was found both at nanograin boundaries and in their interiors. Quasistatic and dynamic nanoindentation tests were carried out on planar polished sections in the range of applied loads from 0.01 to 10 mN. The results were complemented with quantitative modulus mapping of local mechanical properties with 10-nm resolution.

Introduction

Skutterudites are known as excellent thermoelectric (TE) materials [1, 2]. They can be produced from relatively cheap starting materials; they can be used in a wide temperature range and they also show long-term stability and good mechanical performance [3, 4]. The quality of a TE material is characterized by the dimensionless figure of merit *ZT*, dependent on the Seebeck coefficient *S*, temperature *T*, the electrical resistivity ρ and the thermal conductivity λ, consisting of an electronic (λ_e) and a phonon (λ_{ph}) part:

$$ZT = \frac{S^2 T}{\rho\left(\lambda_e + \lambda_{ph}\right)}. \quad (1)$$

Skutterudites already achieved fair efficiency for the conversion of heat to electricity. Researchers are trying to further enhance the figure of merit by various ways, e.g. mechanical alloying and/or nanostructuring [5]. In recent papers by the group in Vienna [6-8] various additives to skutterudites were thoroughly tested with the aim of further increasing *ZT* by shortening phonon free path and thus reducing thermal conductivity without changing electrical resistivity and Seebeck coefficient. Structural, physical and mechanical properties were measured and it was found that namely the small additions of metallic borides proved to increase the thermal-electrical conversion efficiency in a wide temperature range. In addition, boride additives also enhanced the hardness, elastic moduli and fracture resistance [6]. Further beneficial effect of boride additives can be found

in specific cases in better matching of thermal expansion coefficients of p-type and n-type skutterudites [7, 8], which is important for practical applications.

Results of previous work [6-8] summarize effect of various additives and their various amounts on TE and other physical and mechanical properties. Based on the selection from this broad range, we focus here on two materials: an industrial p-type $DD_yFe_3CoSb_{12}$ skutterudite and an industrial n-type $(Mm,Sm)_yCo_4Sb_{12}$ skutterudite, both mixed with 1 wt.% of $Ta_{0.8}Zr_{0.2}B$. DD in the chemical formula denotes didymium (i.e. mixture of Nd and Pr), similarly mischmetal Mm is a mixture of several lanthanides (majority of Ce+La, smaller amounts of Nd, Pr and other trace rare earths). Microstructure of the alloys was studied by means of analytical electron microscopy with emphasis on element distribution. Local mechanical properties were measured at nanoscale by means of nanoindentation experiments.

Experimental

For both, p- and n-type skutterudites ($DD_yFe_3CoSb_{12}$ and $(Mm,Sm)_yCo_4Sb_{12}$) powders produced by Treibacher Industry AG, Austria were used. Stoichiometric amounts of Ta and Zr pieces with a minimal purity of 99.99 mass% and crystalline B powder with a minimal purity of 99.8 mass% all from Alfa Aesar, Germany were arc melted under Ar to produce $Ta_{0.8}Zr_{0.2}B$. The melted pieces were crushed in the glove box and added to the sieved powder of p-type $DD_yFe_3CoSb_{12}$ or n-type $(Mm,Sm)_yCo_4Sb_{12}$. After blending the powders were high energy ball milled and uniaxially hot pressed for 1 h under 56 GPa at 650 °C.

Thin cross sectional lamellae were prepared by FIB (focused ion beam) in a Tescan LYRA 3XMU SEM×FIB scanning electron microscope (SEM). A Philips CM12 STEM transmission electron microscope (TEM) operating at 120kV and a FEI Titan Themis 60-300 cubed high resolution TEM operating at 300kV with a high sensitivity energy dispersive X-ray (EDX) analytical system (0.7 srad solid angle) were then used to study details of microstructure.

Standard metallographic procedures were used to prepare planar polished surfaces for measurements of local mechanical properties; the final polishing was done using a Buehler VibroMet vibratory polisher for 24 h to guarantee the best possible surface smoothness. The hardness and elastic modulus were measured and evaluated by depth sensing nanoindentation technique performed on a Hysitron TI950 Triboindenter equipped with a Berkovich tip. The tip diameter was less than 50 nm. The nanoscale measuring head with resolution of 1 nN and load noise floor less than 30 nN was used for this study. Several testing modes were used in the range of indentation loads from 0.01 to 10 mN, namely quasistatic nanoindentation test, quasistatic nanoindentation with several unloading segments and dynamic modulus mapping in the range from 200 to 300 Hz. The quasistatic indentation tests were carried out in load controlled regime using a constant loading rate of 0.2 mN/s. The partial unloading experiments were carried out in the constant strain rate regime. The standard procedure proposed by Oliver and Pharr [9] was used for the evaluation of the hardness and elastic modulus. For the indentation depths (less than 30nm) a special area function was applied using calibration with low indentation loads [10].

Results and Discussion

The broken surface of the samples was examined with SEM to see the overall microstructure and grain size. SEM micrographs of both samples (Fig. 1) show intercrystalline fracture surfaces of well compacted material with fine equiaxial polyhedral grains (150–400 nm).

TEM observations of thin lamellae prepared by FIB reveal finer details of microstructure. Precipitates are distributed both at grain boundaries (tens of nm in size) and in grain interiors (starting below 10 nm). The situation is qualitatively similar in both samples (Fig. 2).

The observed nanoprecipitates are most probably oxides of rare earths and compounds of other alloying elements coming from borides. Their overall effect on physical and mechanical properties was thoroughly evaluated in recent papers [6-8]. However, for better understanding ongoing processes it would certainly be useful to know what are the phases and what is their preferential

location in the microstructure. XRD could not be used to identify minor phases due to the very small volume fraction of nanoprecipitates. Neither electron diffraction was of help. We collected long term high magnification EDX maps in TEM to see at least qualitatively the elements distribution (Fig. 3 and 4).

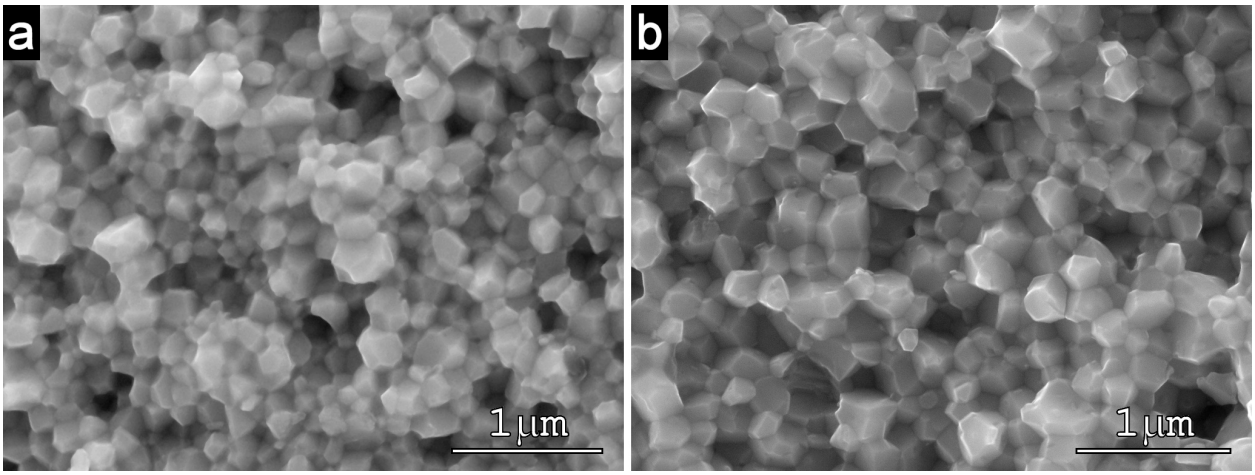

Figure 1. Fracture surfaces of hot pressed powders of $DD_yFe_3CoSb_{12}$+$Ta_{0.8}Zr_{0.2}B$ (a) and $(Mm,Sm)_yCo_4Sb_{12}$+$Ta_{0.8}Zr_{0.2}B$ (b). SEM micrographs, signal of secondary electrons.

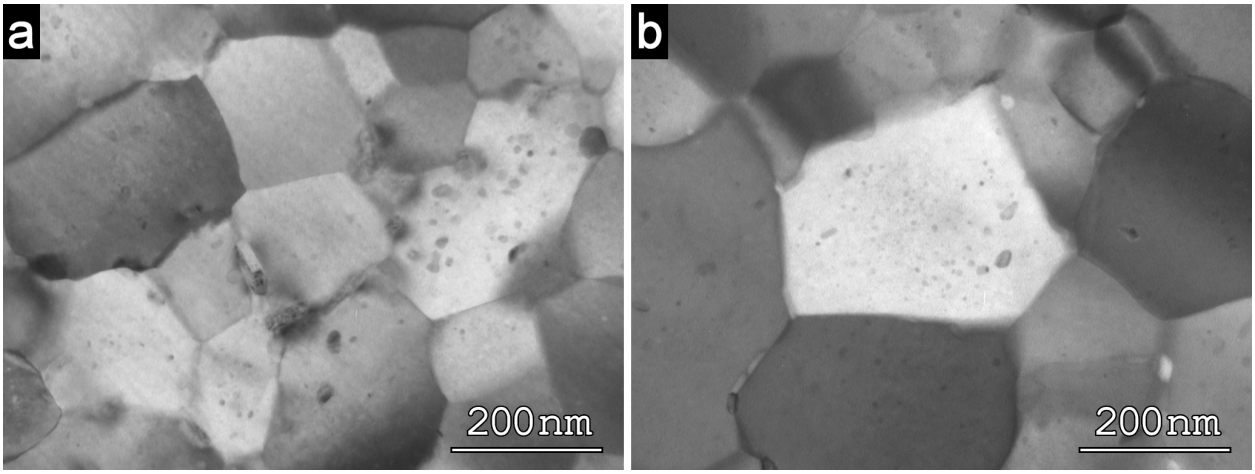

Figure 2. TEM micrographs of grains and distribution of nanoprecipitates in $DD_yFe_3CoSb_{12}$+ $Ta_{0.8}Zr_{0.2}B$ (a) and $(Mm,Sm)_yCo_4Sb_{12}$+$Ta_{0.8}Zr_{0.2}B$ (b).

EDX elemental maps on nanoscale shed some light on the nature of nanoprecipitates and differences between the two alloys. In the DD-containing sample (Nd+Pr)-rich particles enriched also with Ta were found both at grain boundaries (bigger ones) and in grain interiors (smaller ones); Zr was found mostly in fine particles inside grains. The matrix consists of Fe, Co and Sb. In the (Mm,Sm)-containing sample (Sm+Ce)-rich particles were found both at grain boundaries (bigger ones) and in grain interiors (smaller ones); from larger particles we could detect also week signal of minority elements Nd and Pr. Ta-rich particles were placed mostly in grain interiors and a substantially weaker signal of Ta was detected also from larger boundary precipitates. On the other hand, in this sample no gradients were found in Zr distribution, weak Zr signal was detected uniformly as well as the strong signal of matrix elements Co and Sb.

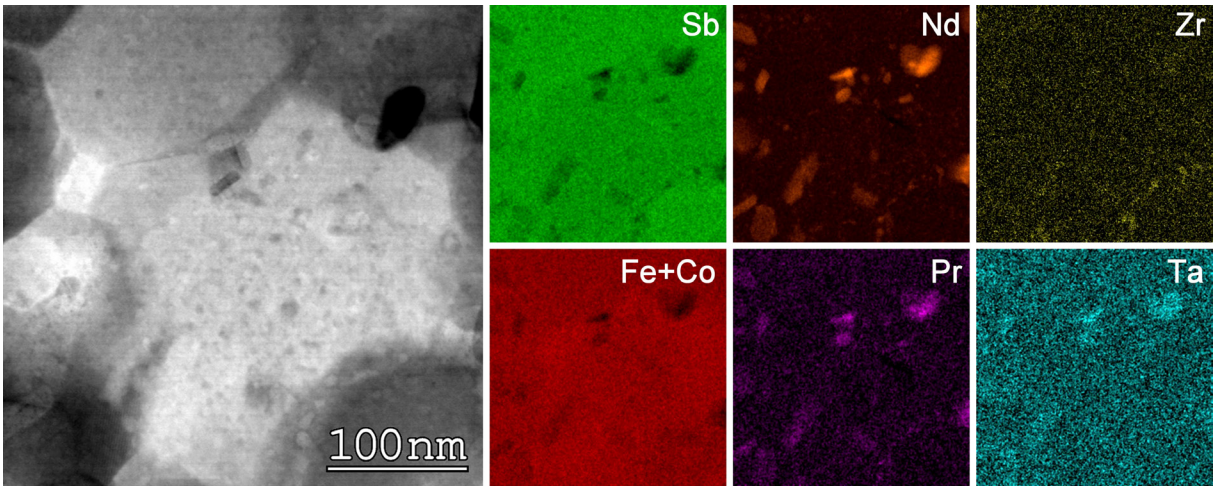

Figure 3. EDX elemental maps collected in TEM showing the distribution of elements in a selected grain in $DD_yFe_3CoSb_{12}$+$Ta_{0.8}Zr_{0.2}B$.

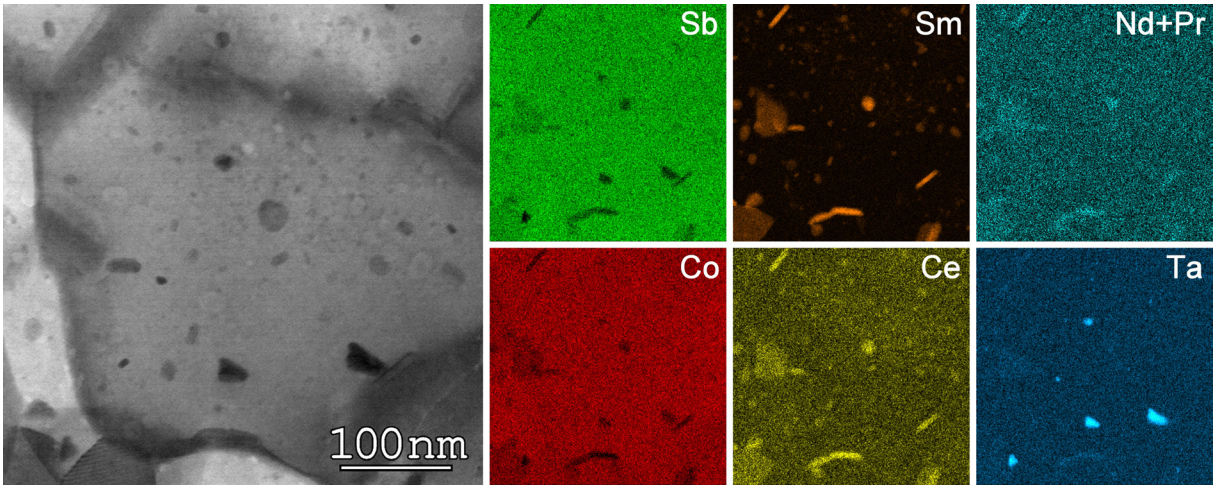

Figure 4. EDX elemental maps collected in TEM showing the distribution of elements in a selected grain in $(Mm,Sm)_yCo_4Sb_{12}$+$Ta_{0.8}Zr_{0.2}B$.

Mechanical properties of $DD_yFe_3CoSb_{12}$ and $(Mm,Sm)_yCo_4Sb_{12}$ with 1 wt.% of $Ta_{0.8}Zr_{0.2}B$ determined using nanoindentation methods are compared in Table 1 with the results of microindentation methods reported previously [7]. The microindentation results were obtained at maximum load of 1N. The nanoindentation results were obtained by means of quasistatic nanoindentation tests using a sharp Berkovich indenter (indenter radius R<50 nm). Around 50 indents were evaluated. The indentation hardness H_{IT} and the reduced elastic modulus E_r were calculated according to the method reported by Oliver and Pharr [9]. The effective elastic modulus was calculated as $E_{eff}=E_rE_i/(E_i-E_r(1-\nu_i^2))$, where E_i and ν_i are the Young's modulus and Poisson's ratio of the diamond indenter, respectively. E^{NI} is Young's modulus estimated from nanoindetation tests as $E^{NI}=E_{eff}(1-\nu^2)$, where ν=0.23 [7]. The results obtained using the nanoindentation method are in good accordance with the microindentation results reported in [7]. There are only slight differences caused by the fact, that in case of the nanoindentation the indentation response of much smaller material volume was studied compared to the microindentation tests. The average hardness values obtained using nanoindentation are slightly higher due to less amount of defects in the deformed volume. However, the differences in Young's moduli are in the frame of the given experimental errors.

The modulus mapping capability was applied to obtain quantitative maps of the storage and loss stiffness. On the basis of these data, the storage and loss modulus maps may be created. The lateral resolution of the modulus mapping method depends on mechanical properties of the measured

material, the nanoindenter tip shape and the settings of the lock-in amplifier which is used to process the displacement signal. In the most simplified approach, the lateral resolution of modulus mapping can be approximated by the size of the contact radius calculated on the basis of Hertz's contact theory [10, 11]. In case of the presented results the estimated lateral resolution was about 10 nm.

Table 1. Mechanical properties of $DD_yFe_3CoSb_{12}$ and $(Mm,Sm)_yCo_4Sb_{12}$ with 1 wt.% of $Ta_{0.8}Zr_{0.2}B$. HV is the Vickers hardness, E^{MI} is the Young's modulus received from microindentation tests (maximum load of 1 N, loading rate of 0.1 N/s and a loading time of 10 s) and ν is Poisson's ratio. E^{MI} and HV values are reported in [7] with experimental error less than 5%. H_{IT} is the indentation hardness and E_r is the reduced elastic modulus, E_{eff} is the effective elastic modulus and E^{NI} is the Young's modulus determined on the basis of the nanoindentation tests (maximum load of 1 mN, loading rate of 0.2 mN/s and a loading time of 5 s).

Sample	HV	E^{MI} [GPa]	ν	H_{IT} [GPa]	E_r [GPa]	E_{eff} [GPa]	E^{NI} [GPa]
$DD_yFe_3CoSb_{12}$ + 1 wt.% $Ta_{0.8}Zr_{0.2}B$	518 [7]	126 [7]	-	6.2±0.5	123±6	137±8	129±7
$(Mm,Sm)_yCo_4Sb_{12}$ + 1 wt.% $Ta_{0.8}Zr_{0.2}B$	711 [7]	143 [7]	0.23[7]	7.5±0.6	135±7	153±9	145±8

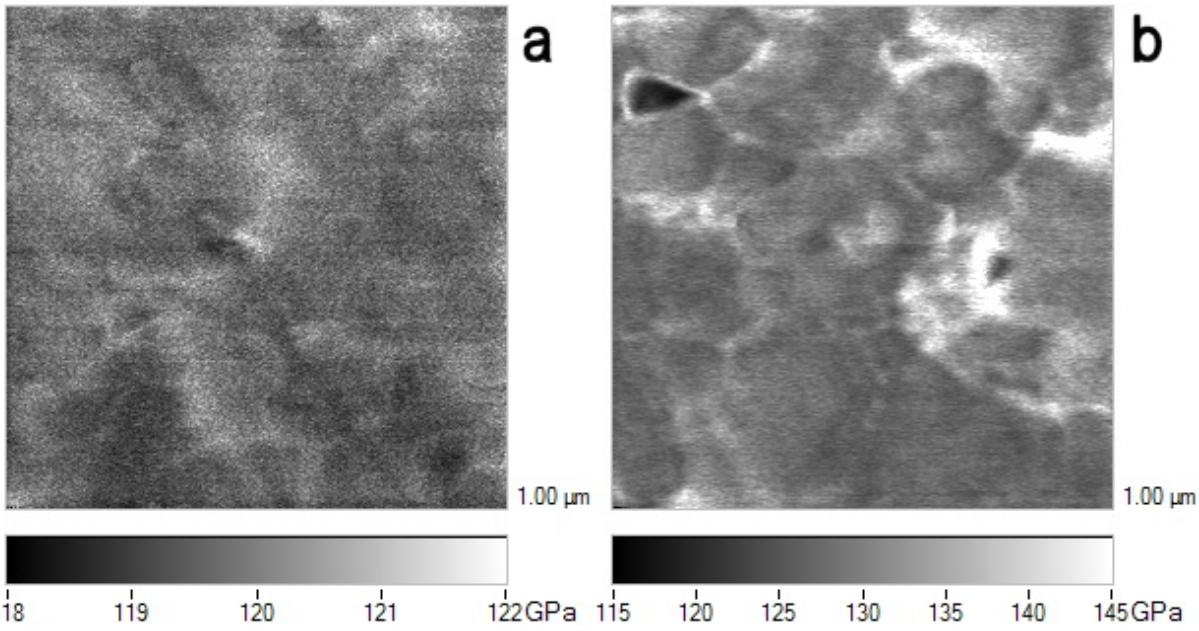

Figure 5. Examples of storage modulus mapping results of $DD_yFe_3CoSb_{12}$ (a) and $(Mm,Sm)_yCo_4Sb_{12}$ (b) with 1 wt.% of $Ta_{0.8}Zr_{0.2}B$. The mapping frequency was 300Hz, the setpoint was 4µN and the oscillation amplitude was 2 µN.

In Fig. 5, examples of storage modulus maps obtained on samples studied at an oscillation frequency of 300Hz and oscillation amplitude of 2 µN are shown. The loss modulus was negligible for both studied samples. The storage modulus maps illustrate the effect of the sample structure on its indentation response. In case of $DD_yFe_3CoSb_{12}$+$Ta_{0.8}Zr_{0.2}B$ sample the modulus map shows small local differences in storage modulus E_{st} (E_{st}=118-122 GPa, Young's modulus obtained from modulus mapping method E^{mm} ~ 124-129 GPa) inside the grains and at their boundaries. The effect of the small (Nd+Pr)-rich particles inside the grain interiors was not distinguishable because their size was lower, than the lateral resolution of the mapping method. In case of the $(Mm,Sm)_yCo_4Sb_{12}$+$Ta_{0.8}Zr_{0.2}B$ sample (E_{st}=115-145 GPa, E^{mm} ~ 121-157 GPa), there are areas with significantly higher storage modulus situated at the grain boundaries which may be associated with the Sm-rich precipitates containing also Nd, Pr and Ce (see Fig. 4). Particles with storage modulus

approx. 115 GPa may be associated with the Ta-rich particles. The average Young's modulus values E^{mm} obtained from modulus mapping method are in good accordance with the results obtained from nanoindentation tests.

Summary

Microstructure and mechanical properties of two thermoelectric materials were studied, namely an industrial n-type $(Mm,Sm)_yCo_4Sb_{12}$ skutterudite and an industrial p-type $DD_yFe_3CoSb_{12}$ skutterudite, both mixed with 1 wt.% of $Ta_{0.8}Zr_{0.2}B$. Thin lamellae were prepared from the compacted materials using a focused ion beam. Analytical transmission electron microscopy was used on lamellae to study details of microstructure. A fine dispersion of precipitates was found both at nanograin boundaries and in their interiors. Quasistatic and dynamic nanoindentation tests were carried out on planar polished sections in the range of applied loads from 0.01 to 10 mN. The results were complemented with quantitative modulus mapping of local mechanical properties with 10-nm resolution.

Acknowledgement

The research has been supported by the Czech Science Foundation (Project 17-12844S). J. Michalička (CEITEC Nano research infrastructure, Brno, Czech Republic) is acknowledged for his help with EDX measurements. G. and P. Rogl gratefully acknowledge the support of the Christian Doppler Laboratory for Thermoelectricity in Vienna, Austria.

References

[1] H.J. Goldsmid, Introduction to Thermoelectricity, Springer-Verlag Berlin, Heidelberg, 2010.

[2] K. Koumoto and T. Mori (Eds.), Thermoelectric Nanomaterials, Materials Design and Applications, Springer-Verlag Berlin, Heidelberg, 2013.

[3] G. Rogl and P. Rogl, Sci. Adv. Mater 3 (2011) 517-538.

[4] L. Zhang, G. Rogl, A. Grytsiv, S. Puchegger, J. Koppensteiner, F. Spieckermann, H. Kabelka, M. Reinecker, P. Rogl, W. Schranz, M. Zehetbauer, M.A. Carpenter, Mater. Sci. Eng. B 170 (2010) 26-31.

[5] G. Rogl and P. Rogl, Current Opinion in Green and Sustainable Chemistry 4 (2017) 50-57.

[6] G. Rogl, A. Grytsiv, F. Failamani, M. Hochenhofer, E. Bauer and P. Rogl, J. Alloys Compd. 695 (2017) 682-696.

[7] G. Rogl and P. Rogl, Materials Today Physics 3 (2017) 48-69.

[8] G. Rogl, J. Bursik, A. Grytsiv, S. Puchegger, V. Soprunyuk, W. Schranz, X. Yan, E. Bauer, P. Rogl, Acta Mater. 145 (2018) 359-368.

[9] W.C. Oliver, G.M. Pharr, J. Mater. Res. 19 (2004) 3-20.

[10] I. Zlotnikov, E. Zolotoyabko, P. Fratzl, Progress in Materials Science 87 (2017) 292–320.

[11] K.L. Johnson, Contact mechanics. Cambridge University Press, 1985.